Int. J. Electrochem. Sci., 12 **(2017)** 3153 – 3165, doi: 10.20964/2017.04.35

International Journal of
ELECTROCHEMICAL
SCIENCE
www.electrochemsci.org

Electrochemical Performances of Maricite $NaFePO_4$/C as cathode material for Sodium-Ion and Lithium-Ion Batteries

Ling Zhao[1], *Dengmei Zhou*[1], *Wanxia Huang*[1,*], *Xueya Kang*[2, 3], *Qiwu Shi*[1], *Zhilin Deng*[3], *Xianwei Yan*[3], *Yongbo Yu*[3]

[1] College of Materials Science and Engineering, Sichuan University, Chengdu 610065, China
[2] Xinjiang Technical Institutes of Physics and Chemistry, Chinese Academy of Sciences, Urumqi, Xinjiang 830011, China
[3] Sichuan Guorun New Mterials Co.,Ltd, Meishan 620010, China
[*]E-mail: huangwanxia@scu.edu.cn

Received: 23 November 2016 / *Accepted:* 13 February 2017 / *Published:* 12 March 2017

Carbon-coated $NaFePO_4$ ($NaFePO_4$/C) with a maricite structure was synthesized by a two-step solid-state method with sucrose as carbon source. The electrochemical performances of $NaFePO_4$/C were evaluated for sodium-ion batteries (SIBs) and lithium-ion batteries (LIBs), respectively. For SIBs, the initial reversible capacity of 48.8 mAh g^{-1} at 0.05 C (1 C=154 mAh g^{-1}) has obtained. For LIBs, the initial discharge capacity of $NaFePO_4$ can reach up to 75.7 mAh g^{-1} at 0.05 C. The reversible capacity of 50.6 and 38 mAh g^{-1} can be obtained at 0.1 C, 0.2 C, respectively. With a simple synthetic process**,** cost-effective chemicals, and desirable electrochemical performance, the maricite $NaFePO_4$/C is a possible application for large-scale energy devices and stationary storage.

Keywords: $NaFePO_4$, maricite, carbon coating, cathode, sodium-ion batteries, lithium-ion batteries

1. INTRODUCTION

Recently, sodium ion batteries (SIBs) have attracted increasing attention. Although lithium ion batteries (LIBs) are now the most common and predominant power source for high power density applications, such as home electronics and mobile electronics [1]. There are several significant challenges facing LIBs for their application in grid-scale ESSs, such as the cost of the fabrication and the raw materials of LIBs, the insufficient energy storage and unevenly distribution. While based on the abundance and easy accessibility of Na, far lower prices, a greener synthesis, and maintained a similarity in ion insertion chemistry, SIBs are more promising candidates for commercialized large-scale energy devices and stationary storage [1−3]. Furthermore, sodium has a suitable redox potential

($E^0_{(Na+/Na)}$ = −2.71 V versus the standard hydrogen electrode), which is only 0.3 V above that of lithium, meaning there is only a small energy penalty to pay. Among the different kinds of electrode materials, iron-based cathode materials ($NaFePO_4$, $Na_4Fe_3(PO_4)_2(P_2O_7)$, $Na_2Fe_{0.5}Mn_{0.5}P_2O_7$ and Na_2FePO_4F [4-6] have been attracting more attention. In particular, the $NaFePO_4$ has the highest theoretical specific capacity (154 mAh g^{-1}) [4-10], which makes it an attractive cathode material for SIBs.

Unlike $LiFePO_4$, the $NaFePO_4$ exists in two distinct polymorphs (triphylite and maricite) [11]. The triphylite $NaFePO_4$, a structural analogue of $LiFePO_4$, offers one dimensional channels for desodiation and sodiation. It has been investigated as a possible cathode for SIBs and delivers a reversible discharge capacity exceeding 120 mAh g^{-1} with an Fe^{3+}/Fe^{2+} redox activity around 3 V [12, 13]. But it is not stable and can only be synthesized by chemical or electrochemical Li-Na exchange process, making triphylite $NaFePO_4$ a less attractive rival for the matching LIBs [14]. The latter is more thermodynamically stable. And its crystal lattice is composed of FeO_6-FeO_6 octahedron by sharing edge, and it is tied by neighboring PO_4 units by sharing corner, offering narrower channels for Na^+ movement [11]. Thus it remains a practical challenge to have an ideal electrochemical performance for maricite $NaFePO_4$. However, surging researches have been carried out on maricite $NaFePO_4$ with insight into its electrochemical performance in recent years. Meanwhile, the non-lithium containing cathode material, such as, Na_2FePO_4F [21], $Na_3V_2(PO_4)_2F_3$ [22] and $NaVPO_4F$ [23] have recently been considered as promising cathode materials for lithium-ion batteries [29]. Thus it is meaningful to further study the electrochemical performance of maricite $NaFePO_4$ for SIBs and LIBs, despite the fact that the electrochemical performance of $NaFePO_4$ is far from optimized at present.

Solid-state reaction is a commonly used method to prepare electrode materials because it is simple and suitable for mass production. And carbon coating has been a successful trial in the solid state processes to enhance its electrochemical performance. In this paper, we would like to use solid-state method to synthesize the maricite $NaFePO_4$ with sucrose as carbon source and further investigate the electrochemical performance of $NaFePO_4$/C for SIBs and LIBs, respectively. The materials were characterized by thermogravimetry and differential scanning calorimetry (TG-DSC), X-ray diffraction (XRD), scanning electron microscopy (SEM), and energy dispersive spectroscopy (EDS). Na-half cells and Li-half cells were subjected to galvanostatic charge and discharge cycles and cyclic voltammetry tests to determine their electrochemical performance and kinetic response.

2. EXPERIMENTAL

2.1. Material synthesis

$NaFePO_4$ sample was synthesized by a two-step solid-state method from the components Na_2CO_3, $FeC_2O_4{\cdot}2H_2O$ and $NH_4H_2PO_4$ in the 0.5:1.0:1.0 (stoichiometric) molar ratio, which was then milled with ethanol solution for 6 h by ball milling. Then, the as-obtained precursor was dried under vacuum followed by pre-sintered at 350 °C for 5 h. And then the precursor was ground and sintered at 650 °C for 10 h with a heating rate of 5 °C min^{-1} to obtain the material. All these heat treatments were conducted under a nitrogen atmosphere to avoid the oxidation of Fe^{2+}. From this mixture five different

compositions were synthesized: (i) without addition of sucrose powder, referred to as $NaFePO_4$, (ii) by the direct addition of sucrose powder of 8 wt.%, 10 wt.%, 12 wt.%, 14 wt.%, referred to as $NaFePO_4$/C@8, $NaFePO_4$/C@10, $NaFePO_4$/C@12, $NaFePO_4$/C@14, respectively. Sucrose was added into raw materials before the ball-milling process.

2.2. Material characterization

Thermogravimetric behavior was carried out on a thermogravimetry and differential scanning calorimetry (TG-DSC) (NETZSCH 409 PC) from room temperature to 800 °C at a heating rate of 10 °C min^{-1} at nitrogen atmosphere. Phase identification and crystal structure analysis were conducted by X-ray diffraction (X' Pert, Philips) with Cu $K\alpha_{1,2}$ radiation (λ= 0.15418 nm) for 2θ between 10° and 80°. The morphological analysis of the particles was investigated by emission scanning electron microscopy (Hitachi S-4800). The chemical components of coating surface were determined by energy dispersive spectrometer (EDS).

2.3. Electrochemical tests

The electrochemical performance of $NaFePO_4$/C was evaluated using CR2032 type coin cells. To fabricate the electrodes, the prepared samples were mixed with polyvinylidene fluoride (PVDF) binder and acetylene black (AB) at a weight ratio of 8:1:1 using N-methylpyrrolidone (NMP) as solvent. Then the resulting slurry was evenly cast onto Al foil with a thickness of 14 μm. After drying under vacuum overnight, the electrodes were punched into wafers with diameters of 14 mm. The loading density of the electrode was ca. 2.5-3 mg cm^{-2}. The coin cells were assembled in an argon-filled glove box using the $NaFePO_4$ as the cathode for both Na and Li half-cells. The Na half-cell was assembled with a Na metal as the reference and counter electrode, and 1 M $NaPF_6$ in ethylene carbonate/dimethyl carbonate solution (volume ratio of 1:1) as electrolyte, a glass fiber as the separator. The Li half-cell was made of a Li metal, a mesoporous membrane Celgard 2400 polypropylene and 1 M $LiPF_6$ in ethylene carbonate (EC)/diethyl carbonate (DEC) (1:1 in volume). Galvanostatic charge-discharge tests at various current densities were carried out using a NEWARE BTS-5 V 10 mA battery tester between 1.5-4 V. The cyclic voltammetry tests were recorded over the potential range of 1.5 V and 4 V using CHI660E electrochemical workstation at a scanning rate 0.05 mV s^{-1}.

3. RESULTS AND DISCUSSION

3.1. TG–DTG analysis of $NaFePO_4$/C

Fig. 1 shows the TG/DSC curves of the precursor of $NaFePO_4$/C, which is useful to determine the decomposition and crystallization temperatures. The first weight loss is about 4.59 wt.% within the

temperature range of 20 °C to 120 °C, corresponding to an endothermic peak at 98.9 °C in DSC curve (peak I in Fig. 1). It can be attributed to the removal of adsorbed water. The second step from 120 °C to 190 °C corresponding to an exothermic peak (peak II in Fig. 1) at 149.8 °C, it was caused by the dehydration process of $FeC_2O_4 \cdot 2H_2O$ [25, 26]. The weight loss was 6.78 wt.%. Afterwards, there was a fall in weight (8.36 wt.%) with an endothermic peak (peak III in Fig. 1) up to 226.8 °C within the temperature range of 190 °C to 369.2 °C. The carbonization of sucrose, the decomposition of FeC_2O_4 and $NH_4H_2PO_4$ were occurred in this temperature zone [24-26]. The last temperature interval with two exothermic peaks (peak IV and peak V in Fig. 1) within the range of 369.2 °C to 464.2 °C can be assigned to the crystallization and the grain growth of the prepared $NaFePO_4$. Thus, the precalcination temperature of the precursor is determined to be in the range of 200 °C to 400 °C, optimally at 350 °C under nitrogen for 5 h. And the subsequent calcination temperature is determined at 650 °C under nitrogen for 10 h to obtain the $NaFePO_4$ particles with good crystallization.

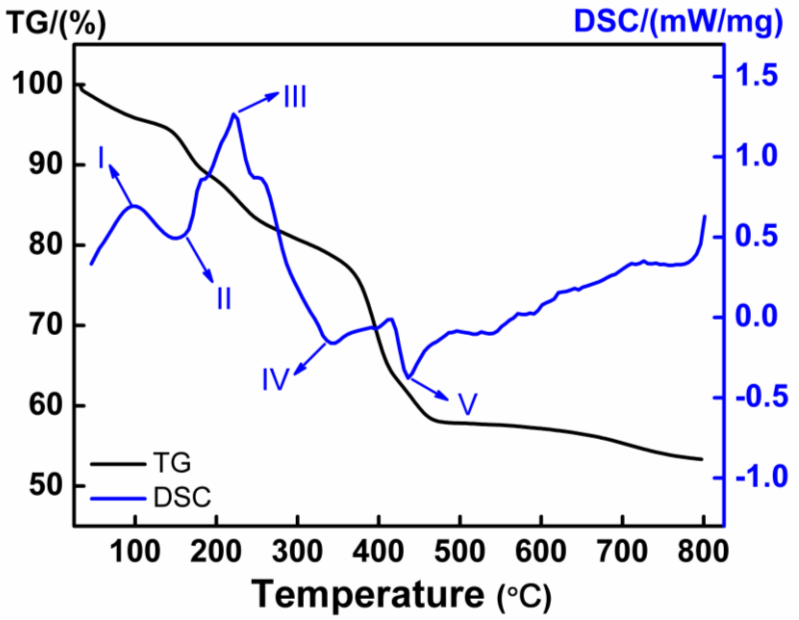

Figure 1. TG/DSC curves of the $NaFePO_4$/C@10 precursor under a nitrogen atmosphere with a heating rate of 10 °C min^{-1}

3.2. XRD and morphology analysis

Fig. 2 shows the X-ray diffraction patterns of $NaFePO_4$ synthesized at 650 °C with different addition of sucrose. All the indexed peaks of the samples match well with the standard patterns of $NaFePO_4$ (JCPDS card number 29-1216), indicating that all samples are maricite $NaFePO_4$ with an orthorhombic structure and a *Pmnb* space group [11]. The crystallite sizes (D) of as-prepared $NaFePO_4$ samples were calculated from the Scherer equation ($D = 0.89\lambda/\beta \cos\theta$) [15], which were calculated according to the three main peaks of (220), (211) and (031) and the lattice parameters (as shown in table 1). With increasing of the pre-adding sucrose content, the average grain size decreases.

Table 1. The full width at half maximum (FWHM) and calculated grain size (D) of the (211), (031) and (222) diffraction peaks for $NaFePO_4$/C with different addition of sucrose

Samples	FWHM(°)		$D_{220, 211}$ (nm)	D_{031} (nm)
	(220)(211)	(031)		
NaFePO4/C	0.311	0.156	35	64
NaFePO4/C@8	0.321	0.163	27	57
NaFePO4/C@10	0.347	0.169	25	55
NaFePO4/C@12	0.349	0.173	24	53
NaFePO4/C@14	0.356	0.176	22	51

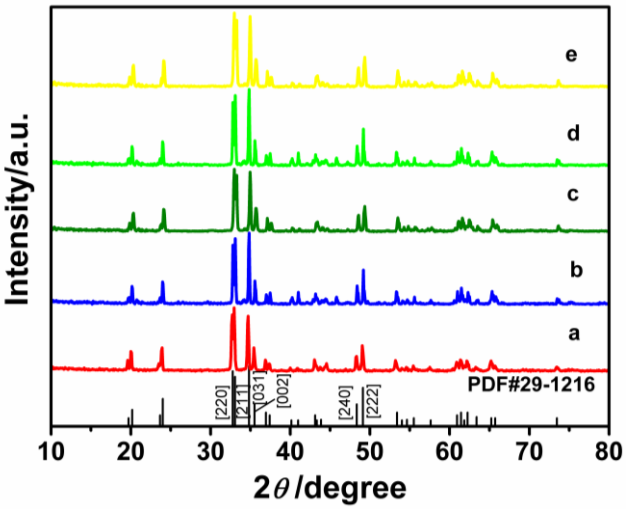

Figure 2. X-ray diffraction patterns of $NaFePO_4$ with different addition of sucrose sintered at 650 °C: **a** bare $NaFePO_4$, **b** $NaFePO_4$/C@8, **c** $NaFePO_4$/C@10, **d** $NaFePO_4$/C@12, **e** $NaFePO_4$/C@14

Fig. 3a-e shows the morphological features of the bare $NaFePO_4$ and $NaFePO_4$/C sintered at 650 °C. The effect of the sucrose contents on the surface morphology of the sample is obvious. The particle size of carbon free $NaFePO_4$ is much larger than that of the carbon coated $NaFePO_4$ particles. With the increased sucrose contents, the particle size of the $NaFePO_4$/C was decreased. It was caused by the pyrolytic carbon from pre-adding sucrose, which inhibited the growth of the particle during sintering process [20, 27]. Compare to the carbon free $NaFePO_4$, $NaFePO_4$/C have more active sites for the electrochemical reaction due to those small dispersed particles, which were distribute on the surface of or among the big particles [30]. And it can be observed from Fig. 3c that with 10 wt.% of the sucrose contents in the synthesis, a better uniformity in size distribution is achieved. Fig. 3f shows the EDX spectra of the $NaFePO_4$/C@10 and it confirmed the existence of carbon.

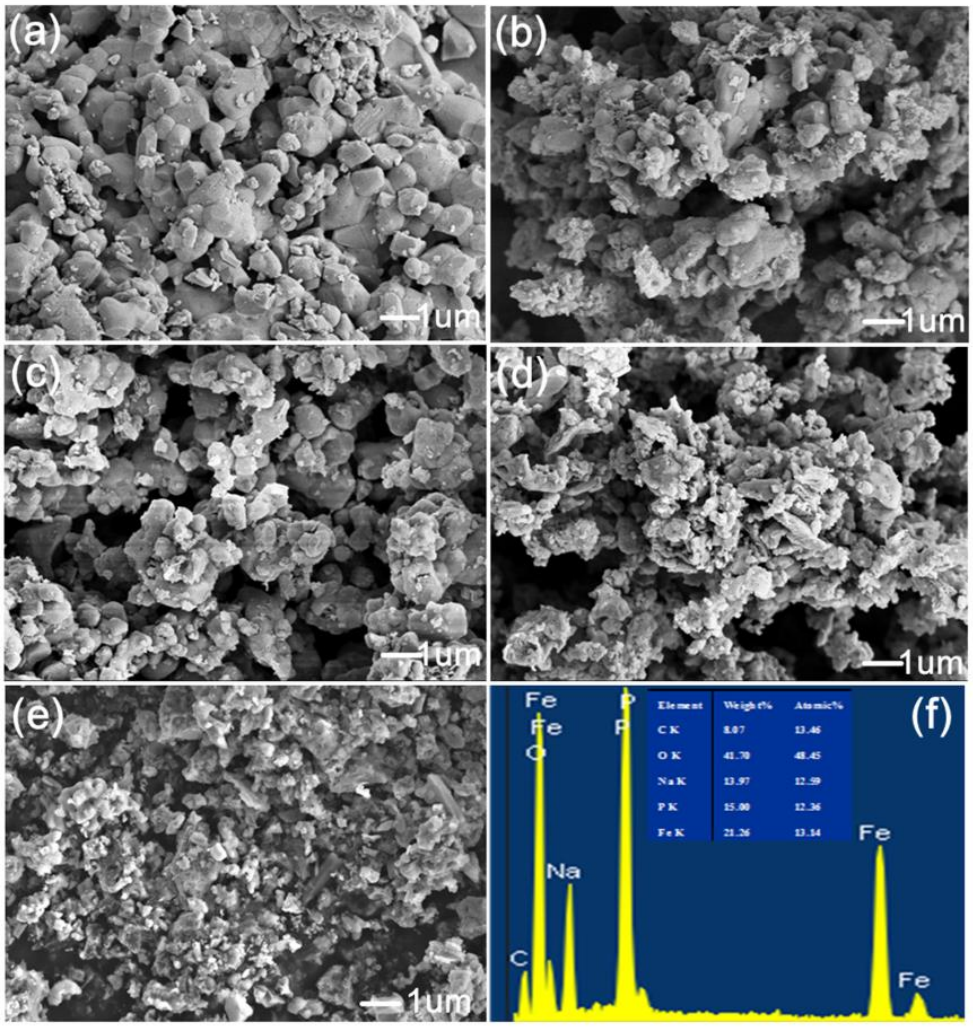

Figure 3. SEM photos of the as-synthesized $NaFePO_4$ powder with different addition of sucrose **(a)** bare $NaFePO_4$, **(b)** $NaFePO_4$/C@8, **(c)** $NaFePO_4$/C@10, **(d)** $NaFePO_4$/C@12, **(e)** $NaFePO_4$/C@14, and **(f)** the EDS spectrum of $NaFePO_4$/C@10

3.3. Electrochemical performance

To further value the electrochemical properties of the $NaFePO_4$ with a maricite structure, the galvanostatic charge-discharge tests at various current densities were carried out in Na-half cells in the potential window 1.5-4 V vs. Na/Na^+. We found the carbon free $NaFePO_4$ was impossible to remove the sodium from the matrix and showed little capacity. It is caused by its low intrinsic electronic conductivity. As shown in Fig. 4, the superiority of $NaFePO_4$/C@10 over $NaFePO_4$/C@8, $NaFePO_4$/C@12 and $NaFePO_4$/C@14 as cathode material is obvious. With the increased charge and discharge rates, the $NaFePO_4$/C@8 and $NaFePO_4$/C@14 show poor performance, and the discharge capacities are only 6.8 and 7.7 mAh g^{-1} at 0.1 C, 5.2 and 6.1 mAh g^{-1} at 1 C (1 C=154 mAh g^{-1}), respectively. The discharge capacity of $NaFePO_4$/C@12 is about 11.6 mAh g^{-1} at 0.1 C. $NaFePO_4$/C@10 shows the best electrochemical performance, delivering a capacity of 17.6 mAh g^{-1} at current rate of 0.1 C. The results proved that the addition of 10 wt.% pre-adding sucrose is the optimal

amount to have preferable conductivity and allow easy sodium ion penetrating. On the one hand, the pyrolytic carbon from pre-adding sucrose can suppress particle growth during the sintering process (as shown in Fig. 3). And it facilitates the formation of fine particles with carbon coating, which will improve the conductivity of $NaFePO_4$/C composite and enhance the electron transport traversing. On the other hand, the smaller particles have the even larger interface, which needs more coated carbon to improve the electronic conductivity of $NaFePO_4$ [27]. So the 10wt.% of the pre-adding sucrose is the optimum amount.

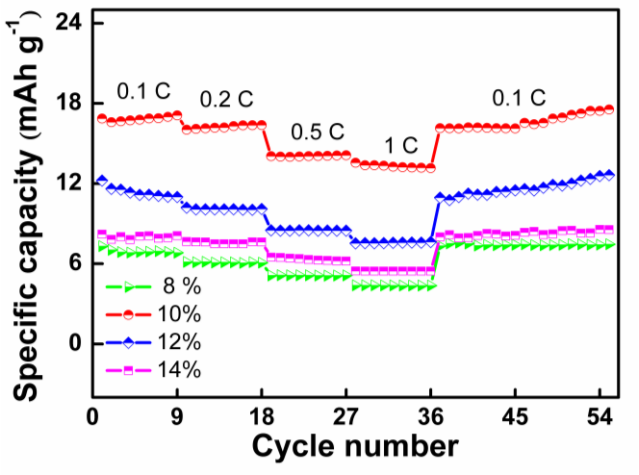

Figure 4. Cycling performance of $NaFePO_4$/C with different carbon contents at different rates varying from 0.1 C to 1 C every 9 cycles

As shown in Fig. 4, it is also clear that after 50 cycles under various conditions, all the $NaFePO_4$/C show increased capacity when the current density is decreased to 0.1 C. It is partially caused by that the initial cycles are helpful to open the closed maricite structure and the strong P-O covalent bond offer chemical and structural stability.

Fig. 5a and Fig. 5b show the cyclic voltammograms of the first two cycles for $NaFePO_4$/C@10 in the potential window 1.5-4 V at a scan rate of 0.05 mV/s tested for Na-half cells and Li-half cells, respectively. Tested for Na-half cells, the CV profile of $NaFePO_4$/C@10 shows one unconspicuous anodic bump and one unconspicuous cathodic bump positioned at 2.52 V and 2.64 V (shown in Fig. 5a), implying a single phase action and sluggish kinitics. Within the first two cycles, the curves exhibit good reversibility with excellent symmetry. The tiny peaks can be explained by that the electrochemical mechanisms upon (de)sodiation suffer from limitations of the radius of Na^+ and that not all the available active mass is involved in the redox processes [28]. However, for $NaFePO_4$/C@10 tested in Li-half cells, two well defined current peaks are found for the cathodic process and only one current peak is observed for the anodic scan (shown in Fig. 5b). The two cathodic peaks observed in Fig. 5b are most likely due to the Li^+/Na^+ mix-insertion mechanism [21, 22, 29, 30], which locate closely at 3.15 V, 2.47 V. It is also clear that the subsequent cycle process exhibits a very similar potential profile to the first charge, indicating a good electrochemical reversibility of the material.

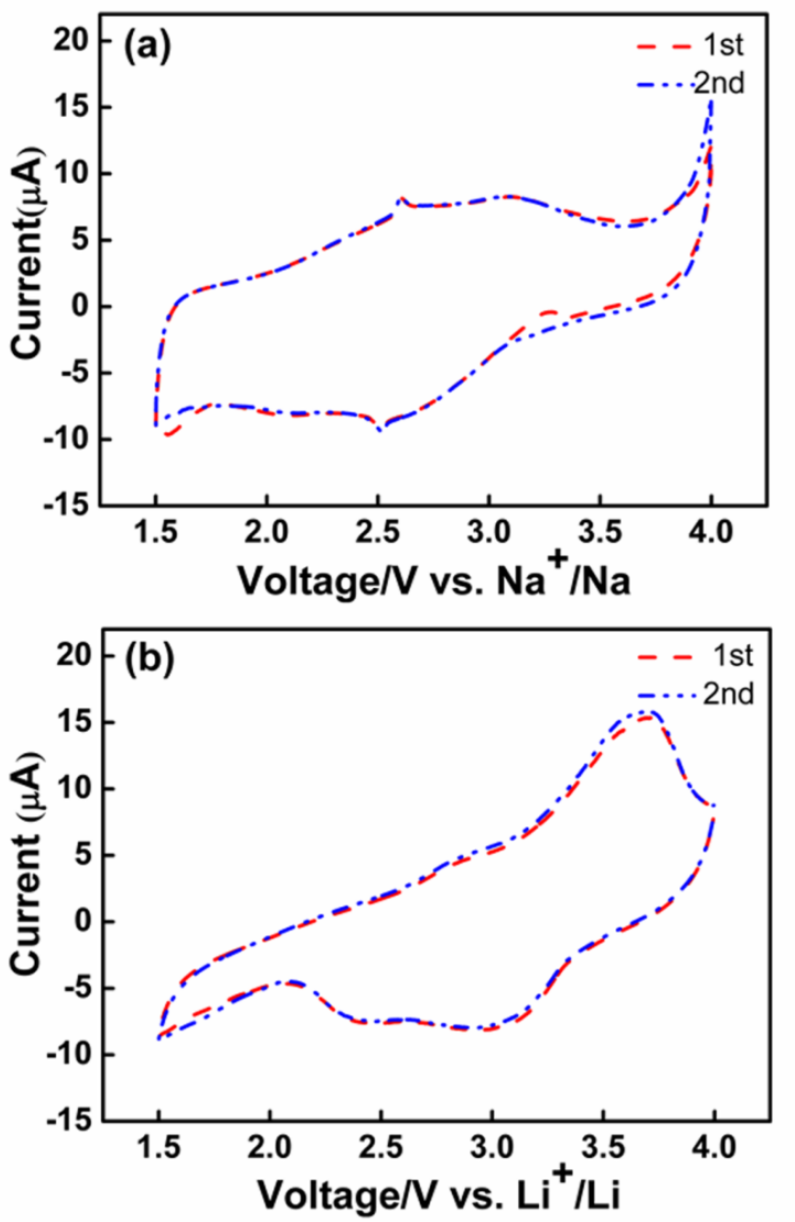

Figure 5. Cyclic voltammograms of $NaFePO_4$/C@10 electrode at the scanning rate of 0.05 mV/s and in a potential window of 1.5-4 V **(a)** vs. Na^+/Na in Na-half cells and **(b)** vs. Li^+/Li in Li-half cells

Fig. 6a-d compares the charge and discharge curves of $NaFePO_4$/C@10 tested in Na-half cells and Li-half cells at various rates. The discharge capacity of $NaFePO_4$/C@10 in Na-half cells is about 48.8, 17.2, 15.9, 14.1 and 13.37 mAh g^{-1} at current rates of 0.05, 0.1, 0.2, 0.5 and 1 C, respectively. This performance is much less than the values of nano-sized maricite $NaFePO_4$ [18, 19], however it is comparable to the values reported in the literature [15-17]. While the discharge capacity of $NaFePO_4$/C@10 in lithium cells is about 75.7, 50.6, 40.9, 34.4 and 14.4 mAh g^{-1} at 0.05, 0.1 C, 0.2 C, 0.5 C and 1 C, respectively. In the Li-half cells, The $NaFePO_4$ showed excellent rate capability. It delivered a high charge capacity of 75.7 mAh g^{-1} at 0.05 C, which was much higher than that of the Na-half cell (48.8 mAh g^{-1}) as shown in Fig. 6a and Fig. 6b.

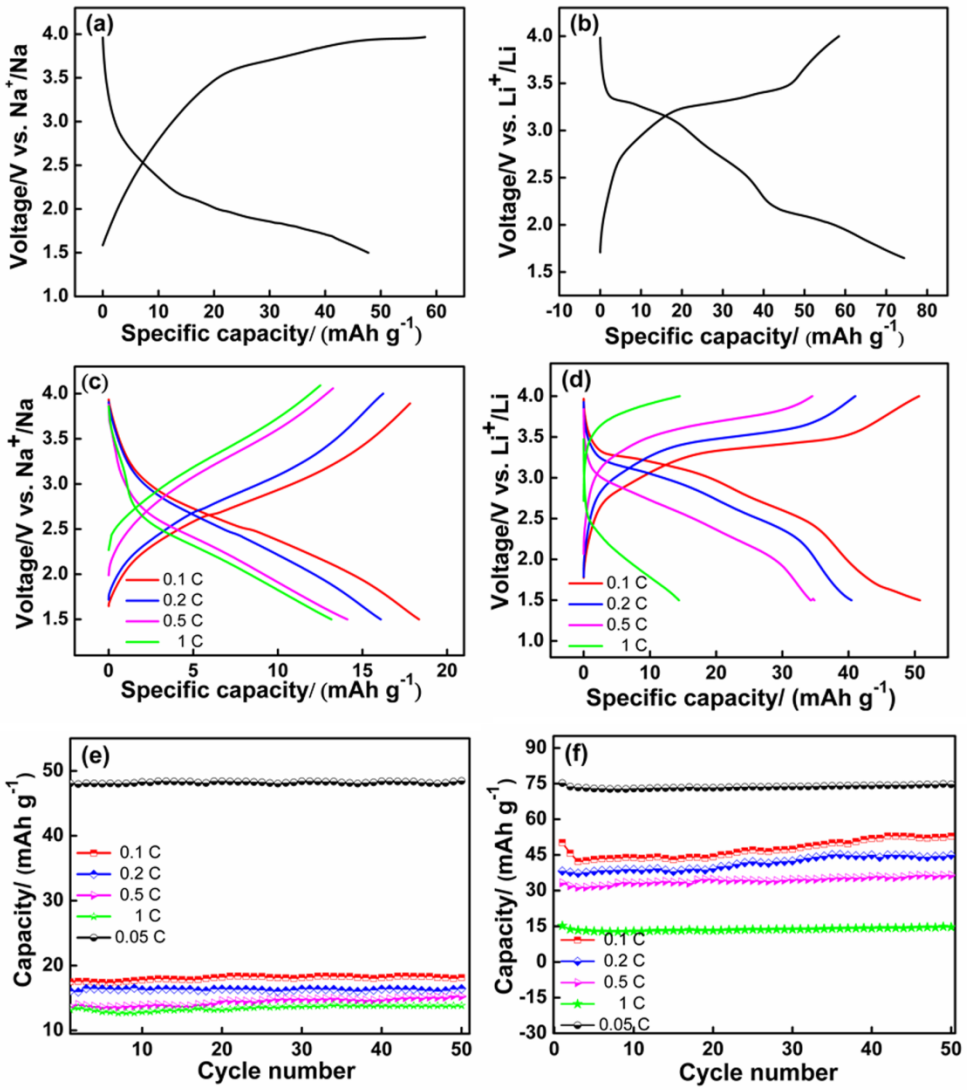

Figure 6. The charge/discharge curves of $NaFePO_4$/C@10 at different C rates **(a)** at 0.05 C in Na-half cells, **(b)** at 0.05 C in Li-half cells, **(c)** from 0.1 C to 1 C rate in Na-half cells, **(d)** from 0.1 C to 1 C rate in Li-half cells; electrochemical cycling at various C rates for $NaFePO_4$@10 tested in **(e)** Na-half cells, **(f)** Li-half cells

The cycling characteristics of the as-prepared $NaFePO_4$/C@10 cathode material at different discharge rate tested in Na-half cells and Li-half cells are shown in Fig. 6e and Fig. 6f. Favorable cycle performance was demonstrated. At all discharge rates, the capacity increase during the 50 cycles in both the Na-half cells and Li-half cells. It implies that the initial cycle is helpful to open the closed maricite structure and the strong P-O covalent bond offers chemical and structural stability. Moreover, the discharge capacities of $NaFePO_4$/C@10 tested in Li-half cells show relatively large increase over the first 50 cycles from 50.6 mAh g^{-1} to 52 mAh g^{-1} and 38 mAh g^{-1} to 41 mAh g^{-1} at 0.1 C, 0.2 C respectively. This phenomenon can be explained by three possible reasons as follows. Firstly, Li^+ ion is much smaller than Na^+ (76 pm vs. 102 pm). Thus, Li^+ is much easier to insert and extract. Secondly, Li^+ ions collaborate with some Na^+ for extraction and insertion leading to more ions participation in its

work mechanism [20-24]. Furthermore, the contribution of the new phase might be helpful for increase in capacity, which will be discussed in the following parts.

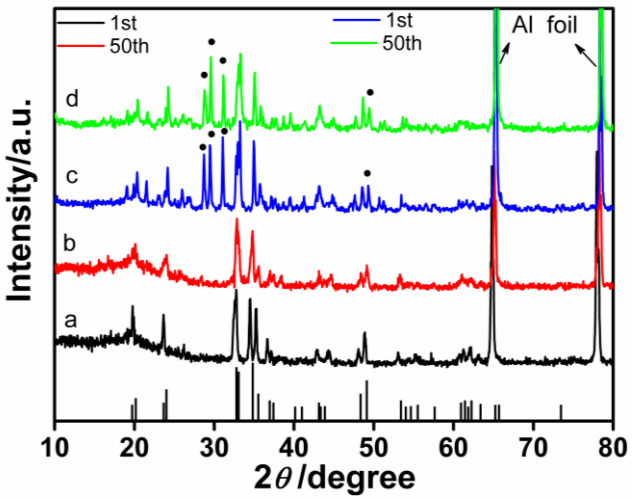

Figure 7. XRD patterns of $NaFePO_4$/C@10 cathode tested in Na-half cells **a** after first cycle, **b** after 50 cycles; tested in Li-half cells **c** after first cycle, **d** after 50 cycles

Table 1. The electrochemical performances of maricite $NaFePO_4$ from recent reports

Ref this work	Synthetic method	The size and the morphology	The cathode tested for	Discharge capacity (mAh g^{-1})		
				0.05C	0.1 C	1 C
12	Hydrothermal route	Prismatic shape Submicro-sized	SIBs	Poor performance		
16	Pechini process	Not reported	LIBs	12 to18 mAh g^{-1} at 5mA/g for 100 cycles		
17	Hydrothermal route	Needles-like micro-sized	LIBs	—	36-38	—
17	Solid-state synthesis	Not reported	SIBs	52	19	—
			LIBs	—	36-38	—
18	Situ hard template method	Hollow amorphous nano-sized	SIBs	—	147.8	124.6
19	Solid-state method	particle size: *ca.*50 nm	SIBs	142	—	90

To confirm the structural changes occurring in the cathode during cycling, the electrode samples were investigated by XRD. Fig. 7a and Fig. 7b show XRD pattern of $NaFePO_4$ for Na-half cell collected separately after the first cycle and the 50th cycle. It is seen that the orthorhombic structure of the sample with *Pnmb* space group maintained unchanged, which is consistent with its structure

stability and pretty well cycling performance. The XRD pattern of $NaFePO_4$ for Li-half cell collected separately after the 1st and the 50th cycle at a current density of 0.1 C are depicted in Fig. 7c and Fig. 7d, respectively. The orthorhombic structure of the sample with *Pnmb* space group is still maintained. However, all reflections are shift to larger angles, indicating a partial Li^+ substitution for Na^+. And it should be noted that there are some low intensity miscellaneous peaks in the XRD patterns. It was caused by Li^+ incorporation and the formation of new phase, which seems to have influence on the capacity for the subsequent consecutive cycles (as shown in Fig. 6). Thus, it can be concluded that after the first cycle in Li-ion cell, the $NaFePO_4$ cathode transforms into the mixed phase and further cycle with Li^+/Na^+ mixed (de)intercalation mechanism.

To date, there are a few reports about the electrochemical performance of the maricite $NaFePO_4$ until now, which can be indexed in Table 2. Most recently, Chun Li [19] reported that hollow amorphous $NaFePO_4$ nano-spheres with the maricite structure have excellent electrochemical capacity, which delivers a capacity of 152 mAh/g, and have a capacity of 144.3 mAh/g after 300 cycles. And Kim et al. [18] also demonstrated that the maricite $NaFePO_4$ via a solid-state method delivered a capacity of 142 $mAhg^{-1}$ (92% of the theoretical value) at the first cycle at 1/20 C rate, and showed outstanding cycle ability with a negligible capacity fade after 200 cycles. The outstanding electrochemical features in the two literatures are attributed to its nano-structure and amorphous feature. The maricite $NaFePO_4$ obtained by hydrothermal methods, has a poor electrochemical performance [12]. Sun et al. [16] report an attractive result on the maricite $NaFePO_4$ as cathode materials for a lithium cell, which was synthesized by the pechini process. It exhibited an initial capacity of 25 mAh g^{-1} and an increase in capacity with cycling. And Masci et al. [17] reported that $NaFePO_4$ via a solid-state method showed a capacity of 19 and 34 mAh g^{-1} for SIBs and LIBs at a current of 0.097 mA g^{-1}, respectively. Although the capacity exhibited in this work is higher than the best capacity reported in those micro-sized maricite $NaFePO_4$, it is still insufficient for its practical use in battery. Compared those maricite $NaFePO_4$ in recent reports, it is likely that proceeding toward to minimizing the grain size and forming amorphous feature to further enhance the electrochemical performance of maricite $NaFePO_4$.

4. CONCLUSIONS

We have successfully synthesized maricite $NaFePO_4$/C composite by a sucrose assisted two-step solid-state method. And the maricite $NaFePO_4$/C electrode was evaluated for LIBs and SIBs, respectively. For SIBs, $NaFePO_4$/C delivers a stable discharge capacity of 48.8 mAh g^{-1} at 0.05 C. it demonstrate that sodium can be extracted and reversibly reinserted from sodium iron phosphate with a maricite structure at low discharge rate. For LIBs, the discharge capacity of $NaFePO_4$/C is about 75.7, 50.6, 40.9, 34.4 and 14.4 mAh g^{-1} at 0.05 C, 0.1 C, 0.2 C, 0.5 and 1 C, respectively. After 50 cycles under various conditions, both the sodium and lithium cells have increase in capacity. Although the capacities observed are lower, the long term stability appears to be good. Even though further study is required, these materials could be of interest for large scale energy storage systems. We anticipate

significant improvement on $NaFePO_4$ by using advanced coatings to increase surface conductivity, and by tuning crystallite size/morphology in the future.

References

1. S. P. Ong, V. L. Chevrier, G. Hautier, A. Jain, C. Moore, S. Kim, X. Ma and G. Ceder, *Energy Environ. Sci.*, 4 (2011)3680.
2. S. W. Kim, D. H. Seo, X. Ma, G. Ceder and K. Kang, *Adv. Energy Mater.*, 2 (2012) 710.
3. V. Palomares, P. Serras, I. Villaluenga, K. B. Hueso, J. C. González and T. Rojo, *Energy Environ. Sci.*, 5 (2012) 5884.
4. H. Kim, I. Park, S. Lee, H. Kim, Y. K. Park, Y. U. Park, H. Kim, J. Kim, H. D. Lim, W. S. Yoon and K. Kang, *Chem. Mater.*, 25 (2013) 3614.
5. R. A. Shakoor, C. S. Park, A. A. Raja, J. Shin and R. Kahraman, *Phys. Chem. Chem. Phys.*, 18 (2016) 3929.
6. B. L. Ellis, W. R. M. Makahnouk, W. N. R Weetaluktuk, D. H. Ruan and L. F. Nazar, *Chem. Mater.*, 22 (2009) 1059.
7. P. Barpanda, T. Ye, S. Nishimura, S. C. Chung, Y. Yamada, M. Okubo, H. Zhou and A. Yamada, *Electrochem. Commun.*, 24 (2012) 116.
8. S. Yu, P. Zhang, S. Q. Wu, A. Y. Li, Z. Z. Zhu and Y. Yang, *J. Solid State Electrochem.*, 18 (2014) 2071.
9. Y. Liu, Y. Zhou, S. Zhang, J. Zhang, P. Ren and C. Qian, *J. Solid State Electrochem.*, 20 (2016) 479.
10. B. L. Ellis, W. R. M. Makahnouk, Y. Makimura, F. Toghiill and L. F. Nazar, *Nature mater.*, 6 (2007) 749.
11. M. Avdeev, Z. Mohamed, C. D. Ling, C. D. Ling, J. Lu, M. Tamaru, A. Yamada and P. Barpanda, *Inorg. Chem.*, 52 (2013) 8685.
12. K. Zaghib, J. Trottier, P. Hovington, F. Brochu, A. Guerfi, A. Mauger and C. M. Julien, *J. Power Sources*, 196 (2011) 9612.
13. S. M. Oh, S. T. Myung, J. Hassoun, B. Scrosati and Y. K. Sun, *Electrochem. Commun.*, 22 (2012) 149.
14. J. N. Bridson, S. E. Quinlan and P. R. Tremaine, Chem. Mater., 10 (1998) 763.
15. K. Zaghib, J. Trottier, P. Hovington, F. Brochu, A. Guerfi, A. Mauger and C. M. Julien, *J. Power Sources*, 196 (2011) 9612.
16. A. Sun, F. R. Beck, D. Haynes, J. A. P. Jr, S. R. Narayanan, P. N. Kumta and A. Manivannan, *Mater Sci. Eng., B*, 177 (2012) 1729.
17. P. P. Prosini, C. Cento, A. Masci and M. Carewska, *Sol. Stat. Ionics*, 263 (2014) 1.
18. C. Li, X. Miao, W. Chu, P. Wu and D. G. Tong, *J. Mater. Chem. A*, 3 (2015) 8265.
19. J. Kim, D. H. Seo, H. Kim, I. Park, J. K. Yoo, S. K. Jung, Y. U. Park, A. William, III. Goddard and K. Kang, *Energy Environ. Sci.*, 8 (2015) 540.
20. T. Yu, Z. Wang, F. Yao, Y. Xiong and S. Guan, *Int. J. Electrochem. Sci.*, 11 (2016) 5999.
21. W. X. Song, X. B. Ji, Z. P. Wu, Y. R. Zhu, Y. P. Yao, K. Huangfu, Q. Y. Chen and C. E. Banks, *J. Mater. Chem.*, 2 (2014) 2571.
22. W. X. Song, X. B. Ji, J. Chen, Z. P. Wu, Y. R. Zhu, Y. R. Ye, H. S. Hou, M. J. Jing and C. E. Banks, *Phys. Chem. Chem. phys.*, 17 (2015) 159.
23. J. Zhao, J. He, X. Ding, J. Zhou, Y. Ma, S. Wu and R. Huang, *J. power sources*, 195 (2010) 6854.
24. F.Cheng, W. Wan, Z. Tan, Y. Huang, Z H. hou, J. Chen and X. Zhang, *Electrochimica Acta*, 56 (2010) 2999.
25. X. Yang, D. Liu, X. Xu, X. He and J. Xie, *CrystEngComm*, 15 (2013) 10648.

26. M. Hermanek, R. Zboril, M. Mashlan, L. Machala and O. Schneeweiss, *J. Mater. Chem.*, 16 (2005) 1273.
27. J. Wang and X. Sun, *Energy Environ.*, 5 (2012) 5163.
28. M. Valvo, B. Philippe, F. Lindgren, C. W. Tai and K. Edström, *Electrochimica Acta*, 194 (2016) 74.
29. W. Song, X. Ji, C. Pan, Y. Zhu, Q. Chen and C. E. Banks, *Phys. Chem. Chem. Phys.*, 15 (2013) 14357.
30. G. Li, P. Wu, C. Luo, Q. Cui, G. Wang and K. Yan, *Journal of Energy Chemistry*, *24* (2015) 375.
31. M. Shimizu, H. Usui, K. Yamane, T. Sakata, T. Nokami, T. Itoh and H. Sakaguchi, *Int. J. Electrochem. Sci.*, 10 (2015)10132